Euler Correction Method for Two- and Three-Dimensional Transonic Flows

Thong Q. Dang* and Lee-Tzong Chen†
Douglas Aircraft Company, Long Beach, California

An Euler correction method, based on the Clebsch formulation of the Euler equations, has been developed to improve shock calculations in full-potential methods. In the Clebsch treatment of steady rotational flows, the velocity is decomposed into potential and rotational components, written in terms of scalar functions. The potential part is computed from the continuity equation using a modified version of an existing finite-volume full-potential solver; the rotational parts are determined analytically from the momentum equation based on small perturbation approximations. The solutions obtained for airfoils and wing/bodies are compared with those using the time-marching Euler methods. The agreement between the results obtained using these two approaches is good.

Introduction

SINCE the introduction of the type-dependent, finite-difference relaxation method of Murman and Cole,[1] the transonic flow computational methods for solving the potential equation have been well developed in the past decade. The finite-volume algorithm[2,3] improves the capability to handle complex geometries, while the multigrid technique improves the computational efficiency.[4,5] In addition, progress in three-dimensional grid generation methods,[6] along with the development of higher-order computational schemes,[7] greatly improve the usefulness of the full-potential approach. However, the irrotationality assumption prevents these methods from taking into account the effects of the vorticity field generated downstream of shocks.

Shocks appearing on wing/body configurations in transonic flow generate entropy that diminishes in strength away from these surfaces. Hence, as shown by the Crocco's relation, vorticity is generated behind shocks. In the presence of weak shocks, the potential approximation to the flowfield is adequate, since the entropy jump across a shock is of the third order in the shock strength.[8] However, as the shock strength increases, the vorticity field behind the shock can significantly alter the flowfield predicted by the potential theory. For example, the prediction of shock locations and shock strengths by the full-potential method can be very different from those predicted by the exact inviscid theory, namely the Euler formulation.

A natural way to include the vorticity field downstream of shocks is to solve the Euler equations. Many recently developed methods, such as the finite-volume time-marching Euler algorithms,[9-11] solve for the primitive variables and have been successfully applied to treat three-dimensional; wing/body configurations. However, they cost more computationally and require larger computer memory than the full-potential methods.

An alternative procedure for solving the Euler equations in terms of the primitive variables is to decompose the velocity vector into a potential part and rotational parts, as suggested by Clebsch.[12] The potential part then can be determined from the continuity equation, while the rotational parts can be found from the momentum and energy equations. This approach is attractive because the potential part of the velocity vector can be determined by solving a modified potential equation using the current state-of-the-art, well-proven, and efficient type-dependent relaxation methods. Moreover, since the far upstream flow is irrotational in many applications, the rotational parts of the velocity vector need to be retained only in the region downstream of shocks, resulting in substantial reduction in computer storage requirements. This "hybrid" approach has been applied by several authors to study two-dimensional rotational transonic flows. For example, in the rotational region behind shocks, Tai[13] used the method of integral relations to solve the Euler equations written in terms of the primitive variables, and Sokhey[14] employed a solenoidal component in the expression for the velocity in addition to the potential part to account for the vorticity field.

The Clebsch transformation has been extensively employed in the calculation of three-dimensional rotational flows in turbomachines up to the subcritical flow range using mostly analytical approaches. The method has been successfully developed for computing shear flow,[15-16] wake flows,[17-19], and nonaxisymmetric inlet flows.[20] This transformation also has been applied to internal and external flow problems by Ecer and Akay,[21,22] but their choices for the Clebsch variables were different from those in the previously mentioned work.

This report presents a method of solving the steady Euler equations for airfoils and wing/body configurations in transonic flows with Clebsch variables. The velocity vector is divided into a potential part and rotational parts, written in terms of scalar functions. The potential part is determined from the continuity equation using a modified version of an existing finite-volume full-potential method.[6] The rotational parts are obtained by solving the momentum equation analytically, based on small perturbation approximations. Another approach to decompose the velocity vector is suggested by Hafez and Lovell.[23,24] The method has been applied to compute flowfields about airfoils. The method proposed in this study differs from those proposed by Hafez and Lovell in that it is derived systematically from the exact three-dimensional form of the steady Euler equation. Hence, the method is general and can be extended straightforward from the two dimensions to three dimensions and used to model other rotational

Presented as Paper 87-0522 at the AIAA 25th Aerospace Sciences Meeting, Reno, NV, Jan. 12-15, 1987; received Nov. 16, 1987; revision received Aug. 30, 1988.

*Senior Engineer/Scientist, Aerodynamic Research and Technology; presently Professor, Department of Mechanical and Aerospace Engineering, Syracuse University, Syracuse, NY.

†Section Manager, Aerodynamic Research and Technology.

effects, such as the trailing vortex sheets behind lifting bodies, or to simulate the rotational flowfield behind propellers.[25,26] Moreover, in theory, the method can be easily extended to a full Euler method by solving for the rotational parts numerically.

Theory

In the Clebsch formulation of steady rotational flows, the velocity vector is decomposed into a potential part and rotational parts, written in terms of scalar functions[12]:

$$V = \nabla\phi + \sum_n \sigma_n \nabla\lambda_n \tag{1}$$

Hence, by definition, the vorticity vector Ω is nonzero:

$$\Omega \equiv \nabla \times V = \sum_n \nabla\sigma_n \times \nabla\lambda_n \tag{2}$$

Clearly, in Eq. (2), the divergence-free condition of the vorticity field is automatically satisfied. To determine the flowfield, the Clebsch variables ϕ, σ_n, and λ_n must be chosen so that the equations of motion are satisfied.

For steady flow, the continuity equation is

$$\nabla \cdot (\rho V) = 0 \tag{3}$$

whereas the momentum equation, written in Lamb's form for isoenergetic flow in the absence of body forces, is

$$V \times \Omega = -(a^2/\gamma)\nabla s \tag{4}$$

where ρ is the density, s the entropy, a the speed of sound, and γ the ratio of the specific heats of the flow.

In the present approach, the potential part in Eq. (1) is determined using the continuity equation, Eq. (3), and the rotational parts in Eq. (1) are chosen to satisfy the momentum equation [Eq. (4)]. The entire flowfield then can be computed by solving the governing equations of these Clebsch variables iteratively.

Governing Equations of the Rotational Parts

The rotational parts of the velocity vector defined in Eq. (1) are determined from the momentum equation. A general solution to Eq. (4) is given by

$$\Omega = \Omega_H + \Omega_p \tag{5}$$

Here Ω_H is the homogeneous solution of Eq. (4), namely,

$$V \times \Omega_H = 0 \tag{6}$$

and Ω_p is the particular solution of Eq. (4),

$$V \times \Omega_p = -(a^2/\gamma)\nabla s \tag{7}$$

The homogeneous soluton represents the vorticity component, which is parallel to the velocity vector. For the problem considered here, Ω_H is the trailing vorticity shed behind a wing. In the airfoil case, Ω_H is identically zero. The particular solution represents the vorticity component, which is not parallel to the velocity vector. When shocks appear in the flowfield, vorticity is generated and is represented by Ω_p.

Consider the particular solution Ω_p. Following arguments similar to those in Refs. 15 or 16, the vorticity component associated with the entropy jump across shocks can be expressed as

$$\Omega_p = \nabla\tau \times \nabla s \tag{8}$$

where s is the entropy field and τ is a Clebsch variable not yet defined. Substituting Eq. (8) into Eq. (7), and using the convective property of entropy along streamlines behind shocks

$$V \cdot \nabla s = 0 \tag{9}$$

it can be shown that the governing equation for τ is

$$V \cdot \nabla\tau = a^2/\gamma \tag{10}$$

Conceptually, the Clebsch variable τ is similar to the Darwin-Lighthill-Hawthorne drift function.[27-28] The variation of τ from streamline to streamline is directly connected to the stretching and tipping of the vortex filaments associated with the entropy variation in the flowfield.

Similarly, it can be shown[16,17,19] that the homogeneous solution is

$$\Omega_H = \delta(\xi)\nabla\xi \times \nabla\Gamma \tag{11}$$

where $\xi \equiv y - f(x,z) = 0$ defines the wake surface or the location of the trailing vortex sheet, $\delta(\xi)$ is the Dirac delta function, and Γ is the circulation of the vortex filaments shed by the wing. Note that according to Eq. (11), the trailing vorticity lies in the wake surface and is zero everywhere except on the wake surface. Substituting Eq. (11) into Eq. (6), along with the use of the "wake" boundary condition

$$V_w \cdot \nabla\xi = 0 \tag{12}$$

the condition for zero pressure jump across the wake, including the trailing edge, is obtained

$$V_w \cdot \nabla\Gamma = 0 \tag{13}$$

Here V_w is the mean velocity between the wake upper and lower sides.

Given the velocity field from the previous iteration step, the Clebsch variables s, τ, ξ, and Γ can be updated by, solving Eqs. (9), (10), (12), and (13), respectively.

Governing Equation of the Potential Part

As mentioned earlier, the continuity equation is employed to determine the potential part of the velocity vector. Using the results derived above, the velocity vector can be written as follows:

$$V = \nabla\phi - s\nabla\tau + H(\xi)\nabla\Gamma \tag{14}$$

where H(ξ) is the step functional. Substituting Eq. (14) into Eq. (3) yields

$$\nabla \cdot \{\rho[\nabla\phi - s\nabla\tau + H(\xi)\nabla\Gamma]\} = 0 \tag{15}$$

The density ρ can be related to the local flow properties by means of the isentropic relation and the energy equation

$$\rho = e^{-s}(M_\infty^2 a^2)^{1/(\gamma-1)} \tag{17}$$

$$a^2 = \frac{1}{M_\infty^2} + \frac{\gamma-1}{2}(1-q^2) \tag{18}$$

where q is the magnitude of the velocity vector and M_∞ the freestream Mach number.

Applications

The strategy of this method is to divide the flowfield into a irrotational region and a rotational region, as shown in Fig. 1. The potential formulation described in the previous section is employed in the irrotational region, whereas the Clebsch formulation is adopted in the rotational region. This approach results in considerable savings in computing time and storage for cases where the rotational region is small. At the boundary interfaces between the irrotational and rotational regions, the Rankine-Hugoniot relation, the Kutta, and the "wake" conditions are used to obtain boundary and matching conditions for the Clebsch variables.

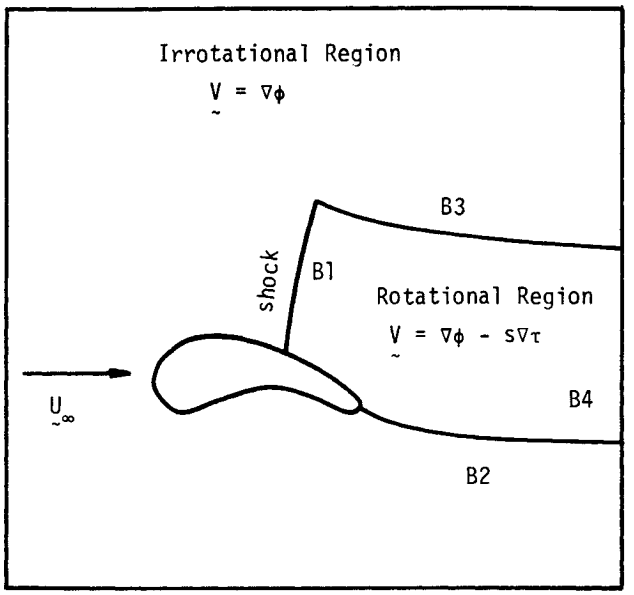

Fig. 1 Irrotational and rotational flow regions.

Airfoil Case

In the airfoil case, there is no trailing vorticity and the expression for the velocity vector in Eq. (14) reduces to

$$V = \nabla\phi - s\nabla\tau \tag{19}$$

In the present method, the governing equation of the potential part is solved numerically, and the governing equations of the rotational part are solved analytically, using small perturbation approximations. These approximations are valid when the contribution of the rotational part in the velocity expression is small (see Appendix A).

First, consider the potential part. In the absence of the trailing vorticity, the governing equation for ϕ, Eq. (16), simplifies to

$$\nabla\cdot(\rho\nabla\phi) = \nabla\cdot(\rho s\nabla\tau) \tag{20}$$

Equation (20) is of the mixed elliptic-hyperbolic type. It is solved using an existing full-potential finite-volume relaxation method[2,6] in the *fully conservative* form, with minor modifications to account for the source term. The modifications required in the potential-flow solver involve computing the residual terms using the new expressions for the density and the velocity given by Eqs. (17) and (19), respectively.

At the boundary interfaces between the irrotational and the rotational regions, the potential function ϕ is chosen to be single valued. Specifically, at the shock front, (interface B1 shown in Fig. 1), the potential function ϕ is chosen to be continuous across the shock. As a result, the conservation of momentum in the direction tangent to the shock front requires the Clebsch variable τ to be a constant everywhere on the shock surface, while the conservation of momentum in the direction normal to the shock front provides the boundary condition for s. At the boundary interface B2, or the streamline emanating from the airfoil trailing edge, the satisfaction of the Kutta and the wake conditions, which require the pressure to be continuous across this streamline, are accomplished by simply keeping the potential jump constant across the branch cut or the grid line emanating from the airfoil trailing edge (see Appendix B). At the boundary interface B3, for the subsonic freestream condition, as the shock strength diminishes from the airfoil surface, the rotational part also vanishes at this boundary, since it is proportional to the entropy jump across the shock. Hence, no special treatment is required at boundary interface B3. Finally, for the two-dimensional case, the far downstream boundary condition for ϕ is specified by using a compressible point-vortex theory, as is extensively used in many potential and Euler airfoil methods.

Next, consider the rotational part. The governing equations for s and τ [Eqs. (9) and (10)] are of the hyperbolic (convective) type. In order to solve them, boundary conditions for s and τ must be prescribed at the shock front. The shock front (interface B1 shown in Fig. 1) is taken to be the surface where the flow changes from supersonic to subsonic. Given the Mach number upstream of the shock and the shock angle, the boundary condition for s can be obtained from the Rankine-Hugoniot relationship. In the present method, for convenience, the entropy is assumed to be convected along the C-type mesh lines (as opposed to the streamlines). Moreover, the speed of sound and the convective speed in the governing equation for τ [Eq. (10)] are assumed to be freestream conditions. Hence, Eq. (10) reduces to

$$(\cos\alpha)\frac{\partial\tau}{\partial x} + (\sin\alpha)\frac{\partial\tau}{\partial y} = \frac{1}{\gamma M_\infty^2} \tag{21}$$

where α is the angle of attack. When these approximations for τ are invoked in the three-dimensional case, the vortex filaments associated with the entropy gradient generated behind shocks are convected with the freestream velocity. This implies that the orientation of these vortex filaments throughout the rotational region remains the same as their initial orientation just behind the shock front, namely, no vorticity distortion, stretching, or tipping occurs.

In order to solve Eq. (21), proper boundary conditions need to be prescribed for τ at the shock front. As mentioned earlier, since the potential function ϕ is taken to be continuous across the shock front requires τ to be a constant everywhere on the shock surface. However, since the Clebsch variable τ itself is not used in the present formulation to compute the velocity, but rather its gradient, this boundary condition is enforced by requiring that the jump in the velocity vector across the shock is normal to the shock surface. Since all of the jump in the velocity across the shock is contained in the rotational part, this condition is satisfied by the following:

$$\nabla\tau\times\hat{n} = 0 \tag{22}$$

where $\hat{n}\equiv(n_x)\hat{e}_x + (n_y)\hat{e}_y$ defines the local shock surface unit normal. Solving Eqs. (21) and (22) simultaneously for the gradient of τ gives, in the two-dimensional case,

$$\nabla\tau = \frac{\hat{n}}{\gamma M_\infty^2(n_x\cos\alpha + n_y\sin\alpha)} \tag{23}$$

Hence, in the two-dimensional Euler correction method, the velocity vector reduces to

$$V = \nabla\phi - \frac{s}{\gamma M_\infty^2(n_x\cos\alpha + n_y\sin\alpha)}\hat{n} \tag{24}$$

To obtain the flowfield, the following iterative procedure is employed:

1) Set the initial solution for ϕ to be the freestream condition, and set s as well as τ to be zero.

2) Solve Eq. (20) for ϕ by a relaxation method.[6]

3) Obtain the shock surface normal vector and the entropy jump across the shocks from the Rankine-Hugoniot relation when supersonic pockets (or shocks) start to appear in the flowfield.

4) Update the rotational part in Eq. (24).

5) Repeat steps 2 to 5 until solutions converge.

Wing Case

In the three-dimensional case, the approach is similar to the two-dimensional case, except for some additional assumptions and modifications. First, the wake or the trailing vortex sheet

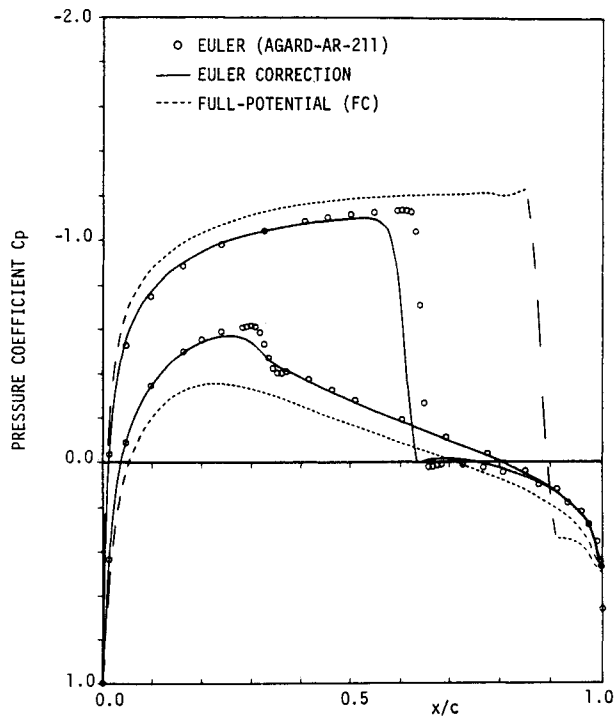

Fig. 2 Comparison of pressure distributions for NACA0012 airfoil at $M_\infty = 0.8$ and $\alpha = 1.25$ deg.

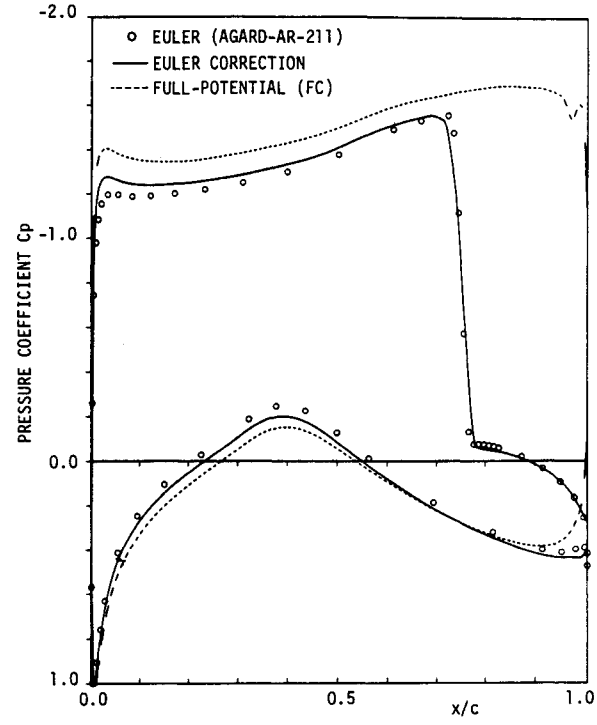

Fig. 3 Comparison of pressure distributions for RAE2822 airfoil at $M_\infty = 0.75$ and $\alpha = 3$ deg.

defined by ξ is taken to be the grid surface emanating from the wing trailing edge. Furthermore, the trailing vorticity is assumed to be convected along the grid lines leaving the trailing edge. This is done by setting the jump in ϕ across the wake at each spanwise station to be constant along the mesh line downstream of the trailing edge. This treatment of the wake is the same as those applied in most potential approaches. Hence, it is not necessary to include the homogeneous solution defined in Eq. (11) into the present method, and the velocity expression simplifies, as in the two-dimensional case, to Eq. (19).

Second, for swept wings, oblique shocks are usually found on most parts of the wing surfaces. In some cases, it is possible to encounter oblique shocks where both the total Mach numbers upstream and downstream of these shock are supersonic. Therefore, the present method of detecting the appearance of shocks in the flowfield described previously is not adequate. This type of shock does appear in many transonic applications, but it is generally weak and, thus, does not require an entropy correction. In the absence of yaw, Eqs. (22–24) still hold in three dimensions where the local shock surface unit normal vector is defined as $\hat{n} = (n_x)\hat{e}_x + (n_y)\hat{e}_y + (n_z)\hat{e}_z$.

Finally, in the three-dimensional case, the Neumann boundary condition is employed in the far downstream region. The implementation of this type of boundary condition requires the knowledge of the far downstream velocity, which is a function of the shock strength. In the present study, the far downstream velocity V_d is taken to be

$$V_d = (\cos\alpha)\hat{e}_x + (\sin\alpha)\hat{e}_y - \frac{s}{\gamma M_\infty^2 (n_x \cos\alpha + n_y \sin\alpha)}\hat{n} \quad (25)$$

where the entropy field s is updated during the calculation.

Conceptually, the last term in Eq. (25) is related to the wave drag and represents the velocity deficit due to the loss in the fluid stagnation pressure across the shock.

Results

In order to assess the accuracy of the present Euler correction method, the solutions obtained for several airfoils and wings using the current approach were compared to those presented in Ref. 29 by the AGARD panel. In the two-dimensional case, a symmetric airfoil (NACA0012) and a supercritical airfoil (RAE2822) were chosen as test cases. The calculations were performed using a 192×32 C-type mesh. In the three-dimensional case, the ONERA-W6 symmetrical swept wing and the NASA swept wing were taken as test cases. Results are also reported for several wing/body configurations that have no Euler solutions to compare against at the present time. The calculations were performed using a $160 \times 24 \times 32$ C-H-type mesh. The results presented in the AGARD report have relatively large discrepancies, particularly the three-dimensional results, because of different numerical schemes, number of grid points, and far-field locations being used; therefore, the most results, accurate solutions, as judged by the AGARD panel, were chosen for comparison in this study.

NACA0012 Airfoil at $M_\infty = 0.8$ and $\alpha = 1.25$ Deg

Figure 2 shows the comparison between the solutions obtained with the present Euler correction approach, the fully conservative full-potential method, and the time-marching Euler calculation reported in Ref. 29. This figure clearly shows that when the rotational part is added to the fully conservative full-potential solution, the resulting C_p distribution moves closer to the time-marching Euler solution. The fully conservative full-potential solution predicts shock locations near the trailing edge and is not well converged. The shocks captured by the Euler correction solution are not as sharp as those obtained by the time-marching Euler solution, especially on the lower surface. This is probably because the time-marching Euler computation employs more points on the airfoil surface than the Euler correction solutions (192 points vs 162 points). The difference in the shock location between the time-marching Euler and the Euler correction solutions is roughly 3% chord. For this test case, this difference is acceptable since the same discrepancies are found between different time-marching Euler solutions, as reported by Rizzi and Viviand.[30] This may be because the NACA 0012 airfoil surface is quite flat in this region.

RAE2822 Airfoil at $M_\infty = 0.75$ and $\alpha = 3$ Deg

This test case was chosen in order to evaluate the accuracy of the Euler correction method in the presence of a strong

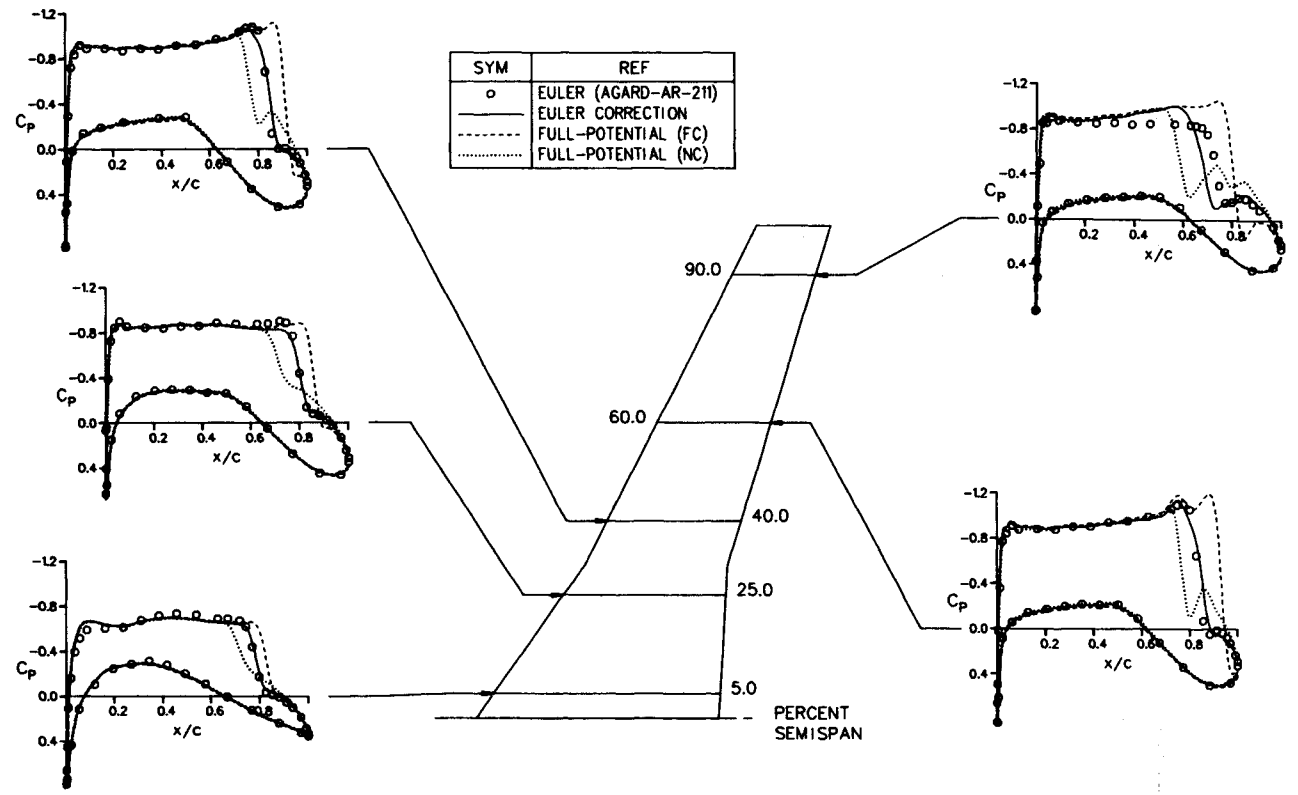

Fig. 4 Comparison of pressure distributions for NASA swept wing at $M_\infty = 0.833$ and $\alpha = 1.75$ deg.

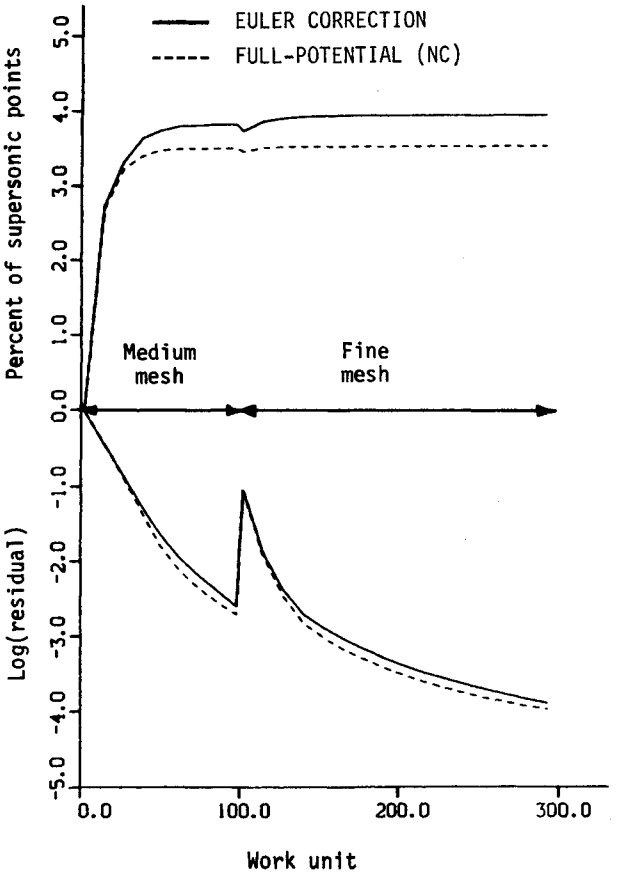

Fig. 5 Comparison of convergence histories for NASA swept wing at $M_\infty = 0.833$ and $\alpha = 1.75$ deg.

shock. Figure 3 gives the C_p comparison between the results obtained using the present Euler correction method, the fully conservative full-potential method, and the AGARD time-marching Euler solution. The overall agreement between the time-marching Euler and Euler correction solutions are excellent, even though this case has a shock Mach number of about 1.7, which is considered to be at the upper limit of the present method according to the analysis shown in Appendix A.

NASA Swept Wing at $M_\infty = 0.83$ and d = 1.75 Deg

This example is a good test case to evaluate the accuracy of the three-dimensional Euler correction method in the presence of strong shocks. The comparison of the pressure distributions at several spanwise stations between the AGARD Dornier/Jameson time-marching Euler solution (the only solution available), the Euler correction solution, and both the fully conservative and nonconservative full-potential solutions is shown in Fig. 4. Note that for this case, the nonconservative full-potential solution converges whereas the fully conservative full-potential solution does not. This figure clearly demonstrates that the Euler correction solution is in excellent agreement with the AGARD Euler solution. On the other hand, the converged nonconservative full-potential solution tends to predict earlier shock formation and weaker shock compared to the time-marching Euler result, whereas the fully conservative full-potential solution exhibits the opposite trend. Moreover, the after-shock re-expansion phenomenon appears in both the nonconservative and the fully conservative full-potential solutions when the shock becomes strong, for example, at the 40 and 60% span locations.

Near the wing-tip region, both the full-potential and the Euler correction methods predict higher suction peak in front of the shock than the time-marching Euler method. Here, large after-shock re-expansion is found in the full-potential solutions, whereas the Euler correction solution does not have this behavior and compares reasonably well with the time-marching Euler solution.

Finally, Fig. 5 shows the convergence histories of average residuals and the percentage of supersonic points in the computational domain as a function of work unit by the nonconservative full-potential and Euler correction methods. This figure demonstrates that the Euler correction method has the

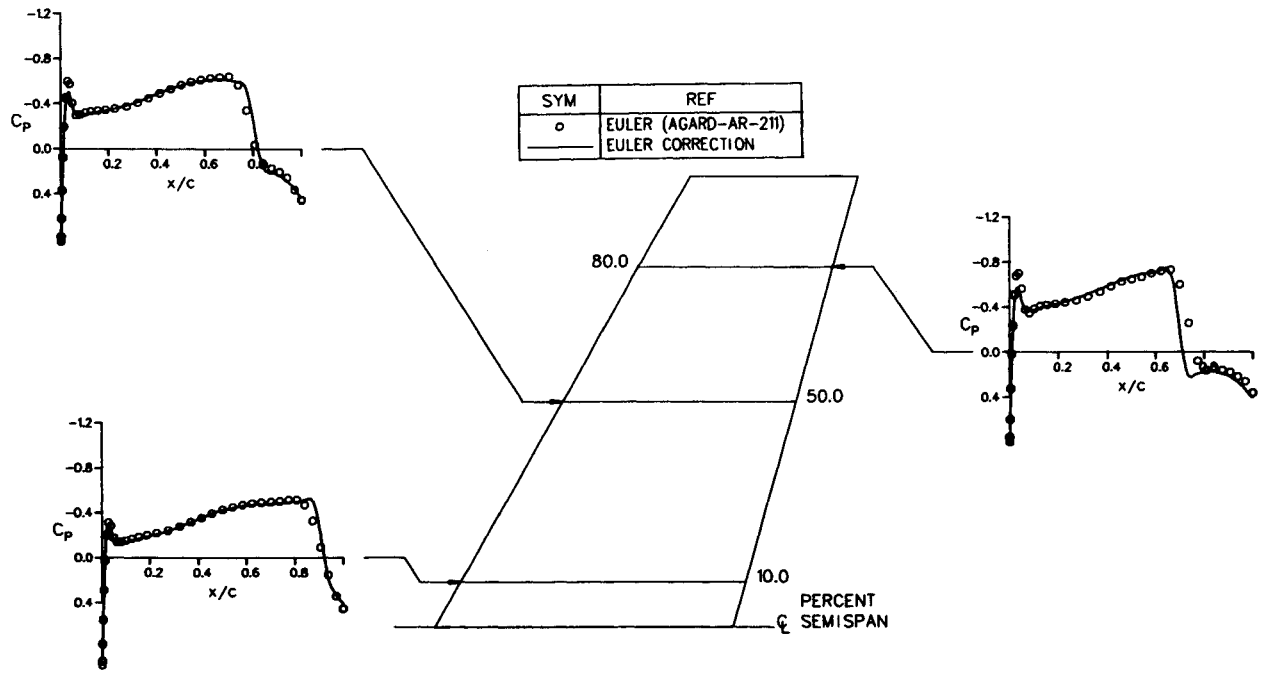

Fig. 6 Comparison of pressure distributions for ONERAM6 wing at $M_\infty = 0.92$ and $\alpha = 0$ deg.

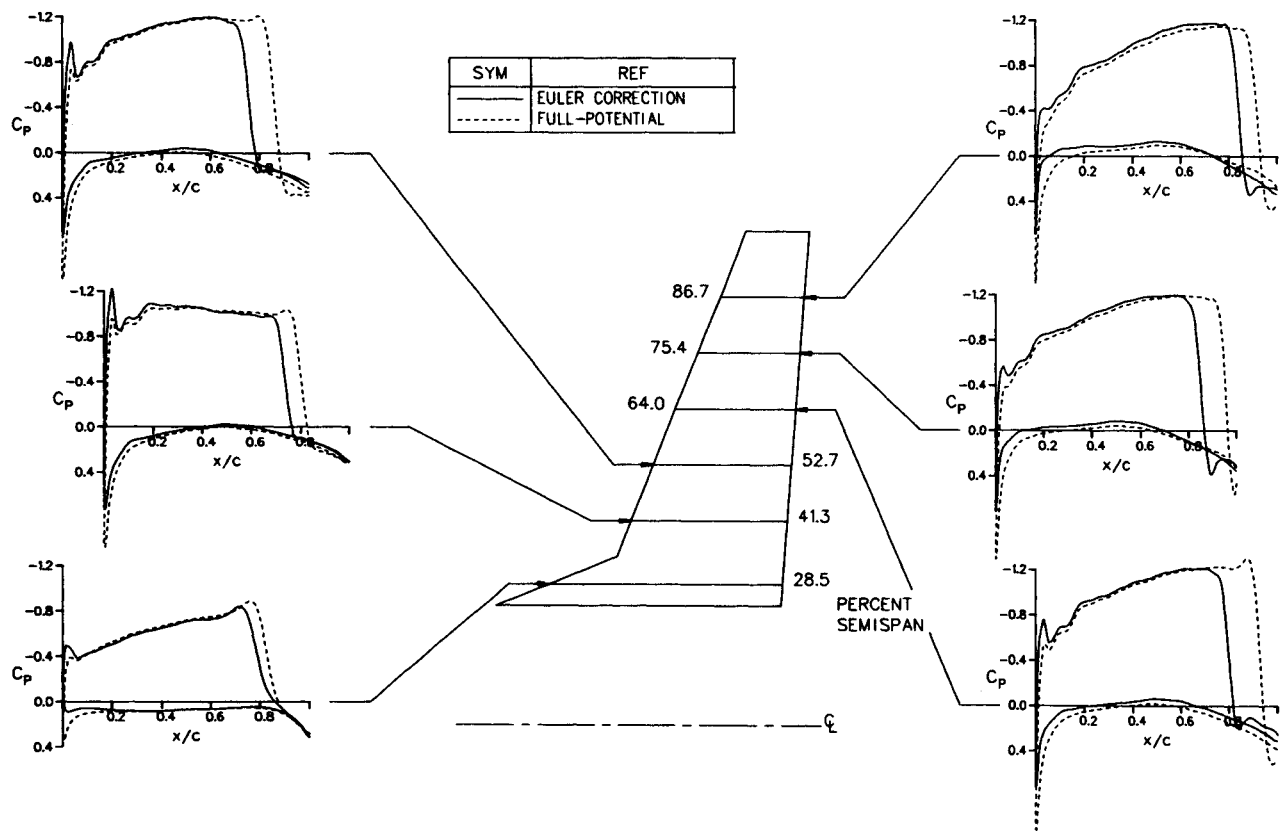

Fig. 7 Comparison of pressure distributions for F-14 wing/body configuration at $M_\infty = 0.85$ and $\alpha = 4$ deg.

same convergence rate as the full-potential method at roughly 20% more in computational time per work unit. On the other hand, the time-marching Euler method is estimated to require roughly one order of magnitude more in computational time over the full-potential method.

ONERAM6 Wing at $M_\infty = 0.92$ and $\alpha = 0$ Deg

At zero degree angle of attack, the ONERAM6 wing is nonlifting. Hence, it does not have a trailing vortex sheet. Inaccurates associated with the poor modeling of the trailing vortex sheet by the present Euler correction method, therefore, can be isolated in this test case. Figure 6 illustrates the comparison of the pressure distributions at three different spanwise locations between the Euler correction solution and the AGARD ONERA/Matra time-marching Euler solution. The AGARD ONERA/Matra solution was chosen for comparison since it lies roughly between the other AGARD solutions and has tabulated C_p data. The full conservative full-potential so-

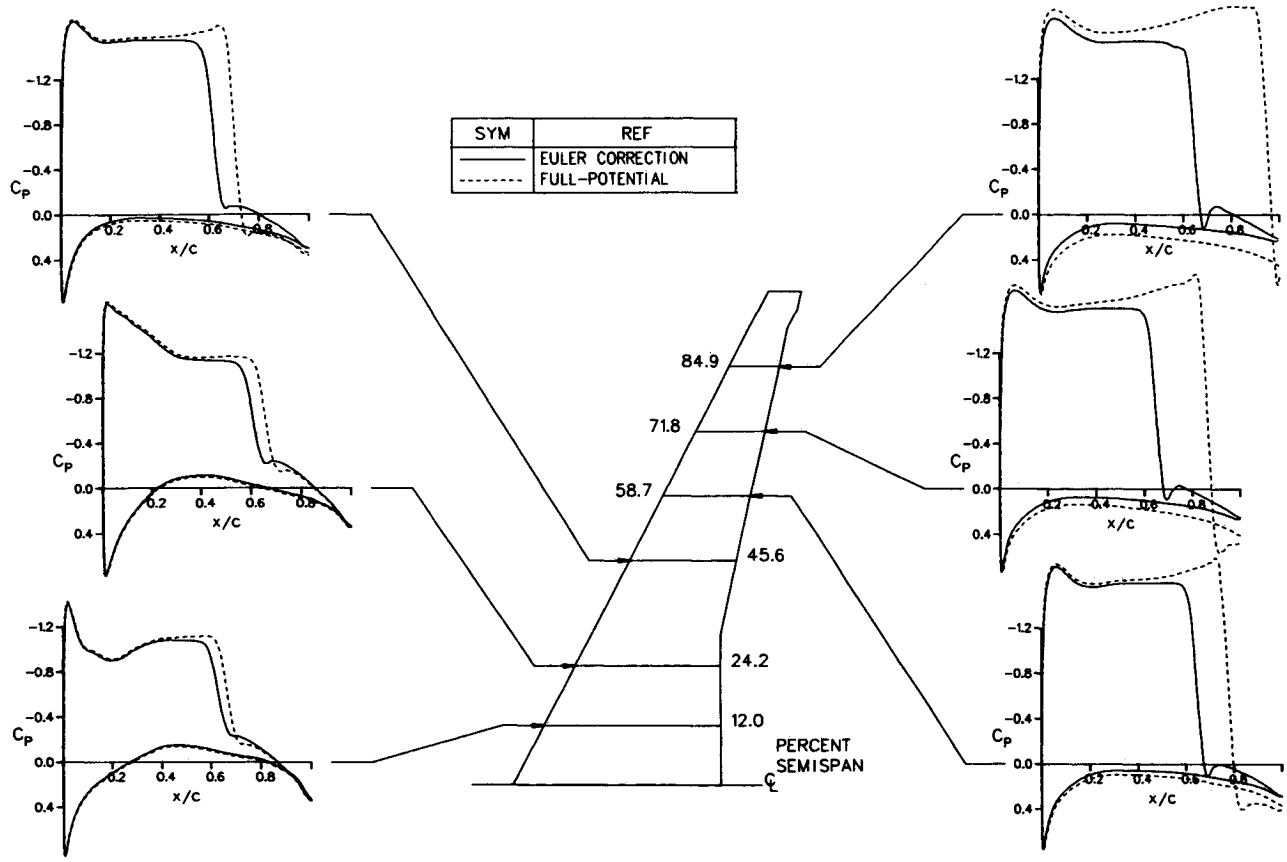

Fig. 8 Comparison of pressure distribution for wing/body configuration at $M_\infty = 0.76$ and $\alpha = 4.2$ deg.

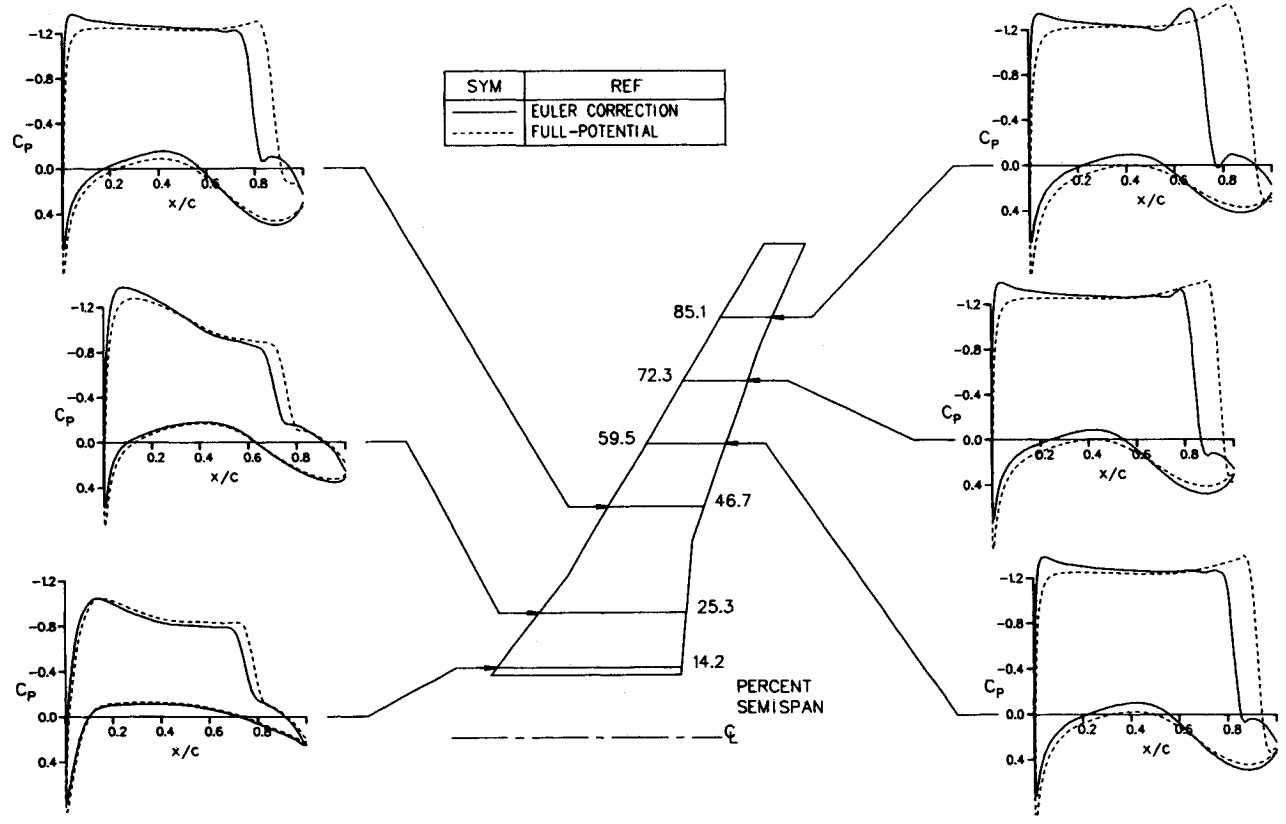

Fig. 9 Comparison of pressure distribution for wing/body configuration at $M_\infty = 0.8$ and $\alpha = 2.3$ deg.

lution is now shown in this figure because it rapidly blows up due to the appearance of a strong shock near the trailing edge in the root region.

As in the previous case, the Euler correction and time-marching Euler solutions are in excellent agreement, except near the wing tip region. Here the Euler correction method predicts the shock location slightly ahead of that predicted by the time-marching Euler method. This discrepancy is very similar to that found in the NASA swept wing case, even though the trailing vortex sheet is absent in this example. Hence, it is

believed that the slight disagreements around the wing-tip region in the results between these methods may be associated with the different ways the wing-tip boundary conditions are handled in these methods.

Wing/Body Configurations

Figures 7-9 show the C_p comparison between the solutions obtained using the Euler correction and the full conservative full-potential methods for three different wing/body configurations. No time-marching Euler solutions are available for these cases, and all three fully-conservative full-potential solutions shown do not converge well under the flow conditions considered because of the presence of strong shocks near the trailing edge. The trends shown by these figures are very similar to the previous two test cases: the Euler correction method gives well-converged solutions by moving the shock location further upstream and by predicting weaker shocks. Note that the small oscillations on the suction surface near the wing leading edge in the F-14 wing/body solution are due to the bad definition of the fuselage geometry, which in turn introduces distorted grid distribution.

Conclusion

An Euler correction method, based on the Clebsch transformation of the steady Euler equations, has been developed to calculate transonic flows around airfoils and wing/body configurations. In this approach, the velocity vector is divided into a potential part and rotational parts, written in terms of scalar functions. The potential part is determined from the continuity equation using a modified version of an existing full-potential method. The governing equations of the rotational parts are obtained from the momentum equation and are solved analytically, based on small perturbation approximations.

Results for several airfoils, wings, and wing/body configurations indicate that the solutions obtained using the present Euler correction method compare well with those obtained using the time-marching Euler method. In particular, the predictions of the shock location and the shock strength agree very well with the time-marching Euler solutions. Furthermore, the computer time required by the Euler correction scheme is about 20% more than that needed by the full-potential method but is estimated to be roughly an order of magnitude less than the computing time required by the time-marching Euler approach.

As the present Euler correction method was derived from the Euler equation, there exist many potential improvements to the method and also a possibility of extending the method into a full Euler method. Possible systematic improvements include the following:

1) The governing equation for the entropy [Eq. (9)] can be solved numerically while keeping the same approximation for the Clebsch variable τ. This implies that the entropy will be convected along the actual streamlines as opposed to the grid lines. This improvement may be useful for high angle of attack cases, and is necessary if grid topologies other than C-grid are employed.

2) In addition to the above, the Kutta and the wake conditions can be satisfied more exactly if the convective speed and the speed of sound in its governing equation are taken to be the local conditions on the airfoil surface and the dividing streamline, as opposed to freestream conditions.

3) In the three-dimensional case, the trailing vortex sheet can be better modeled through the use of Eqs. (12) and (13).

4) Finally, if the governing equations for the rotational parts defined previously are solved numerically and a stable iterative scheme between the potential and rotational parts can be found, the resulting solution is equivalent to an Euler solution.[31]

Appendix A: Order of Magnitude of the Rotational Part

The potential approximation in transonic flow calculations has proven to be a useful design tool in the presence of weak shocks. As the shock strengths increases, the vorticity field generated behind shocks become important. In this Appendix, an order of magnitude study for the rotational part in the velocity expression is presented. In the previous discussion of the Airfoil Case, the velocity expression was shown to be

$$V = \nabla\phi - s\nabla\tau \tag{A1}$$

where the rotational part is $s\nabla\tau$. Given the Mach number upstream of the shock, the magnitude of the entropy jump across the shock can be determined from the Rankine-Hugoniot relationship

$$s = \frac{1}{\gamma - 1}\ell n\left\{\left[\frac{2\gamma}{\gamma+1}M_s^2 - \frac{\gamma-1}{\gamma+1}\right], \left[\frac{(\gamma-1)M_s^2 + 2^\gamma}{(\gamma+1)M_s^2}\right]\right\} \tag{A2}$$

where M_s is the upstream Mach number component normal to the shock surface.

To estimate the magnitude of the Clebsch variable τ, consider its governing equation:

$$V \cdot \nabla\tau = \frac{a^2}{\gamma} \tag{A3}$$

On using freestream conditions for the convective speed and the velocity of sound, Eq. (A3) reduces to

$$\frac{\partial\tau}{\partial x} \sim 0\left(\frac{1}{\gamma M_\infty^2}\right) \tag{A4}$$

Figure A1 shows the order of magnitude of the rotational term based on Eqs. (A2) and (A4) as a function of the shock Mach number and the freestream Mach number. As expected, the order of magnitude of the rotational term increases with increasing shock Mach number. These results also show that the contribution of the rotational part in the velocity expression increases with decreasing freestream Mach number. This study indicates that in typical transonic application, the small perturbation approximation used to compute the rotational part in the present Euler correction method can introduce

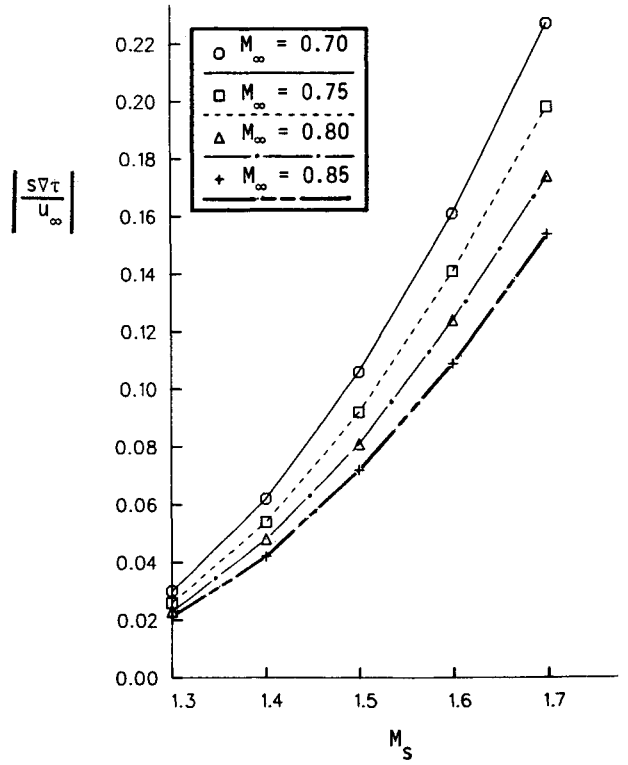

Fig. A1 Order of magnitude of the rotational part vs shock Mach number at various freestream conditions.

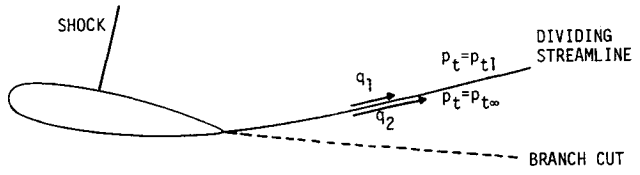

Fig. B1 Notation used in the derivation of the Kutta and the wake conditions.

noticeable error. For example, $|s\,\nabla\tau|/u_\infty$ is of the order of 20% for a shock Mach number of roughly 1.7 or greater. However, numerical experiments have shown that the method works very well even in this range. For example, for the RAE2822 airfoil calculation at $M_\infty = 0.75$ and $\alpha = 3$ deg, where the shock Mach number is approximately 1.7, comparison of the pressure coefficient between the time-marching Euler and the Euler correction solutions are excellent (see Fig. 3).

Appendix B: Kutta and Wake Conditions

The Kutta and the wake conditions require the pressure to be continuous at the airfoil trailing edge and across the streamline emanating from the airfoil trailing edge (or the dividing streamline). In the absence of shock on the airfoil surfaces, the stagnation pressure is constant throughout the flowfield. In this case, the Kutta and wake conditions require the magnitude of the velocity to be continuous at the airfoil trailing edge and across this dividing streamline. When the full-potential formulation is employed, the Kutta and the wake conditions can be satisfied by simply keeping the potential jump constant across the branch cut behind the airfoil trailing edge. Here, the branch cut does not have to coincide with the dividing streamline.

In the presence of shocks on the airfoil surfaces, the stagnation pressure is discontinuous across this dividing streamline. Hence, in order to have equal pressure across the dividing streamline, the velocity must be discontinuous across it. In this Appendix, the velocity deficit across the dividing streamline will be shown to come from the rotational term $s\,\nabla\tau$ in Eq. (19), so that the potential ϕ is continuous across the dividing streamline.

To facilitate the derivation, consider the case where there is a shock on the airfoil upper surface and no shock on the airfoil lower surface (Fig. B1). On using the isentropic relationship, the static pressure can be related to the local velocity and stagnation pressure:

$$p_1 = \left(\frac{p_{t1}}{p_{t\infty}}\right)\left[1 + \frac{\gamma-1}{2}M_\infty^2(1-q_1^2)\right]^{\gamma/\gamma-1} \tag{B1}$$

$$p_2 = \left[1 + \frac{\gamma-1}{2}M_\infty^2(1-q_2^2)\right]^{\gamma/\gamma-1} \tag{B2}$$

The Kutta condition requires the pressure to be equal across the dividing streamlines. Equating Eqs. (B1) and (B2), one obtains

$$\left(\frac{p_{t1}}{p_{t\infty}}\right)\left[1 + \frac{\gamma-1}{2}M_\infty^2(1-q_1^2)\right]^{\gamma/\gamma-1} = \left[1 + \frac{\gamma-1}{2}M_\infty^2(1-q_1^2) - (\gamma-1)M_\infty^2 q_1\Delta q - \frac{\gamma-1}{2}M_\infty^2\Delta q^2\right]^{\gamma/\gamma-1} \tag{B3}$$

where $\Delta q \equiv q_2 - q_1$. Neglecting the term Δq^2 in Eq. (B3), an explicit expression for the velocity deficit across the dividing streamline can be found

$$\Delta q \simeq \frac{1}{q_1}\frac{1}{\gamma M_\infty^2}\left[1 - \left(\frac{p_{t\infty}}{p_{t1}}\right)\right]\left[1 + \frac{\gamma-1}{2}M_\infty^2(1-q_1^2)\right] \tag{B4}$$

In practice, the stagnation pressure loss across the shock is generally small even for a strong shock. For example, a shock Mach number of 1.7 results in 15% loss in stagnation pressure. Since Δq is proportional to the stagnation pressure loss, the assumption of neglecting the Δq^2, term in deriving Eq. (B4) is valid.

If the velocity deficit is completely accounted for by the rotational part, then it must be true that

$$\Delta q = \left(s\frac{\partial\tau}{\partial\ell}\right)_1 \tag{B5}$$

where ℓ is the distance measured along the dividing streamline. The righthand side of Eq. 5 can be related to the local velocity and stagnation pressure via the use of the governing equations for the rotational part.

For isoenergetic flow, the entropy is related to the stagnation pressure by

$$s = -\ell n\left(\frac{p_{t\infty}}{p_{t1}}\right) \simeq 1 - \left(\frac{p_{t\infty}}{p_{t1}}\right) \tag{B6}$$

where, as before, second-order terms in the stagnation pressure loss are neglected.

From the governing equation of the Clebsch variable τ [Eq. (10)]

$$\frac{\partial\tau}{\partial\ell} = \frac{1}{q_1}\frac{1}{\gamma M_\infty^2}\left[1 + \frac{\gamma-1}{2}M_\infty^2(1-q_1^2)\right] \tag{B7}$$

Substituting Eqs. (B6) and (B7) into Eq. (B5), one obtains

$$\Delta q \simeq \frac{1}{q_1}\frac{1}{\gamma M_\infty^2}\left[1 - \left(\frac{p_{t\infty}}{p_{t1}}\right)\right]\left[1 + \frac{\gamma-1}{2}M_\infty^2(1-q_1^2)\right] \tag{B8}$$

Clearly, Eqs. (B4) and (B8) are identical. Hence, the velocity deficit across the dividing streamline required to satisfy the Kutta and the "wake" conditions is completely contained in the rotational part of the velocity vector. As a result, the boundary condition for ϕ across the branch cut is the same as in the full-potential method. Again, the location of the branch cut does not have to coincide with the dividing streamline.

Acknowledgments

This research was supported in part by the Naval Ship Research and Development Center under Contract N00167-85-C-0134, and in part by the McDonnell Douglas Independent Research and Development program.

References

[1]Murman, E. M. and Cole, J. D., "Calculation of Plane Steady Transonic Flows," *AIAA Journal,* Vol. 9, Jan. 1971, pp. 114–121.

[2]Jameson, A. and Caughey, D. D., "A Finite-Volume Method for Transonic Potential-Flow Calculations," *Proceedings of the AIAA 3rd Computational Fluid Dynamics Conference,* AIAA, New York, June 1977, pp. 35–54.

[3]Caughey, D. A. and Jameson, A., "Numerical Calculation of Transonic Potential Flow About Wing-Body Combinations," *AIAA Journal,* Vol. 17, Feb. 1979, pp. 175–181.

[4]Jameson, A., "Acceleration of Transonic Potential Flow Calculations on Arbitrary Meshes by the Multiple Grid Method," AIAA Paper 79-1458, July 1979.

[5]Shmilovich, A. and Caughey, D. A., "Application of the Multi-Grid Method to Calculations of Transonic Potential Flow About Wing-Fuselage Combinations," NASA SP-2202, Oct. 1981, pp. 101–130.

[6]Chen, L. T., Vassberg, J. C., and Peavey, C. C., "A Transonic Wing-Body Flowfield Calculation with an Improved Grid Topology," *AIAA Journal,* Vol. 23, Dec. 1985, pp. 1877–1884.

[7]Chen, L. T., "A More Accurate Transonic Computational Method for Wing/Body Configurations," *AIAA Journal,* Vol. 31, June 1983, pp. 848–855.

[8]Shapiro, A. H., *The Dynamics and Thermodynamics of Compress-*

ible Fluid Flow, Wiley, New York, 1953.

[9]Jameson, A., Schmidt, W., and Turkel, E., "Numerical Solutions of the Euler Equations by Finite Volume Methods Using Runge-Kutta Time-Stepping Schemes," AIAA Paper 81-1259, June 1981.

[10]Steger, J. L., "Implicit Finite-Difference Simulation of Flow About Arbitrary Geometries with Application of Airfoils," AIAA Paper 77-665. Jan. 1977.

[11]Rizzi, A., "Damped Euler-Equation Method to Compute Transonic Flow Around Wing-Body Combinations," *AIAA Journal,* Vol. 20, Oct. 1982, pp. 1321–1328.

[12]Lamb, H., *Hydrodynamics,* Dover, New York, 1960.

[13]Tai, T. C., "Hybrid Approach to Transonic Inviscid Flow with Moderate to Strong Shock Wave," *Transonic Aerodynamics,* edited by D. Nixon, Vol. 21, *Progress in Astronautics and Aeronautics,* NY, AIAA, 1982.

[14]Sokhey, J. S., "Transonic Flow Around Axisymmetric Inlets Including Rotational Flow Effects," AIAA Paper 80-0341, Jan. 1980.

[15]Hawthorne, W. R., "On the Theory of Shear Flow," Massachusetts Institute of Technology, Cambridge, MA, MIT GTL Rept. 88, 1966.

[16]Dang, T. Q., "A Three-Dimensional Blade Design Method to Control Secondary Flow," Ph.D. Thesis, Dept. of Aeronautics and Astronautics, Massachusetts Institute of Technology, Cambridge, MA, June 1985.

[17]McCune, J. E. and Hawthorne, W. R., "The Effects of Trailing Vorticity on the Flow Through Highly-Loaded Cascades," *Journal Fluid Mechanics* Vol. 74, April 1976, pp. 721–740.

[18]Chen, L. T. and McCune, J. E., "Comparison of 3-D Quasi-Linear Large Swirl Theory with Measured Outflow From a High Work Compressor Rotor," Massachusetts Institute of Technology, Cambridge, MA, MIT GTL Rept. 128, 1975.

[19]Tan, C. S., "Vorticity Modeling of Blade Wakes Behind Isolated Annular Blade Rows: Induced Disturbances in Swirling Flows," *ASME Journal of Engineering for Power,* Vol. 103, No. 2, April 1981.

[20]Hawthorne, W. R., McCune, J. E., Mitchell, N. A., and Tan, C. S., "Nonaxisymmetric Flow Through an Annular Actuator Disk: Inlet Distortion Problem," *ASME Journal of Engineering for Power,* Vol. 100, 1978.

[21]Ecer, A. and Akay, H. U., "A Finite Element Formulation f Euler Equations for the Solution of Steady Transonic Flows," *AIAA Journal,* Vol. 21, 1983, pp. 343–350.

[22]Akay, H. U., Ecer, A., and Willhite, P. G., "Finite Element Solutions of Euler Equations for Lifting Airfoils," *AIAA Journal,* Vol. 24, 1986, pp. 562–569.

[23]Hafez, M. and Lovell, D., "Entropy and Vorticity Correction for Transonic Flows," AIAA Paper 83-1926, 1983.

[24]Hafez, M. and Lovell, D., "Transonic Small Disturbance Calculations Including Entropy Correction," *Numerical and Physical Aspects of Aerodynamic Flows, II,* Springer-Verlag, New York, 1984.

[25]Dang. T. Q., "Simulations of Propeller Effects Using an Actuator Disk and the Euler-Clebsch Method," Douglas Aircraft Co., Rept. MDC J4953, Dec. 1987.

[26]Chen, L. T., Yu, K. C., and Dang, T. Q., "A Transonic Computational Method for An Aft-Mounted Nacelle/Pylon Configuration with Propeller Power Effect" AIAA paper 89-0560, Jan. 1989.

[27]Lighthill, M. J., "Drift," *Journal of Fluid Mechanics,* Vol. 1, Pt. 1, 1956, pp. 31–53. Note also "Corrigenda to Drift," *Journal of Fluid Mechanics,* Vol. 2, 1957, pp. 311–312.

[28]Hawthorne, W. R., "The Actuator Duct Representative of Turbomachinery Blade Rows," Liber Amicorum Andre L. Jaumotte, Inst. of Applied Mechanics, Universite Libre de Bruxelles, TN 50, pp. 1983, 395–405.

[29]"Test Cases for Inviscid Flow Field Methods," AGARD-AR-211, May 1985.

[30]Rizzi, A. and Viviand, H., "Numerical Methods for the Computation of Inviscid Transonic Flows with Shock Waves," *Notes on Numerical Fluid Mechanics,* Vol. 3, GAMM Workshop, Vieweg and John, 1981.

[31]Dang, T. Q. and Chen, L. T., "An Euler Correction Method for Two- and Three-Dimensional Transonic Flows," AIAA Paper 87-522, Jan. 1987.